Cumhuriyet Sci. J., 44(3) (2023) 595-601
DOI: https://doi.org/10.17776/csj.1239911

Cumhuriyet Science Journal

| csj.cumhuriyet.edu.tr | Founded: 2002 ISSN: 2587-2680 e-ISSN: 2587-246X Publisher: Sivas Cumhuriyet University

Synthesis and Characterization of Tb–Er Co–Doped Bi2O3 Solid Electrolyte Systems

Murat Balcı[1, a, *]

[1] *Department of Physics, Faculty of Science, Erciyes University, Kayseri, Türkiye*
**Corresponding author*

Research Article

History
Received: 21/01/2022
Accepted: 31/07/2023

ABSTRACT

In this study, solid state reactions were used to create Er–Tb co–doped Bi2O3 solid electrolyte systems. Four Point Tip Technique (FPPT), Thermo–gravimetric and Differential Thermal Analysis (TG & DTA), and X–Ray Diffraction (XRD) were used to characterize the generated samples' structural and thermal properties, and electrical conductivity. The samples 05Er05TbSB, 05Er10TbSB, and 15Er05TbSB stabilized with cubic δ–phase at room temperature, according to XRD data. Due to the smaller dopants ions compared to the host Bi3+ cation, the lattice constants estimated for these samples were lower than those of the pure cubic phase. The samples were thought to be thermally stable in the studied temperature range since the thermal curves did not show endothermic or exothermic peak development indicating a potential phase change. According to the Arrhenius equation, the temperature–dependent conductivity graphs displayed a linear change. The conductivity measurements clearly indicated that an increase in doping rate results in a sudden drop in electrical conductivity. The calculated activation energies increased with the doping ratio and varied from 0.64 eV to 1.12 eV. At 700 °C, it was determined to be 0.128 $S.cm^{-1}$ for the sample 05Er05TbSB, which had the greatest conductivity and lowest activation energy among all samples. The conductivity was discovered to decrease and activation energy to increase when the doping ratio was gradually raised.

Keywords: Phase Transition, X–Ray Diffraction, Electrical Activation Energy, Electrical conductivity, Solid–State Reaction.

[a] *muratbalci@erciyes.edu.tr* *https://orcid.org/0000–0003–1297–1691*

Introduction

Solid oxide fuel cells (SOFCs) are alternative energy sources that use electrochemistry to create electrical energy. Because it has a higher electrical efficiency output than other fuel cells, this system may be used as an extra source of electricity in standard power units such as hospitals, schools, and companies [1, 2]. However, the SOFC cell's high operating temperature creates several internal challenges. The most serious of them is temperature–related wear (corrosion) at the electrode–electrolyte interfaces, which lowers cell electrical efficiency and reduces battery life [3]. A typical SOFC cell is made up of three basic solid layers. These are the anode, where the fuel gas is oxidized, the cathode, where the oxygen gas is reduced, and the electrolyte layer, which allows the transport of O^{2-} ions from the cathode to the anode boundary [4, 5]. The corrosions cause the solid electrolyte layer to deteriorate, causing the cell to short circuit and the open circuit voltage to decrease dramatically.

Most researchers have also reported internal problems caused by high operating temperature in recent years, and studies have accelerated to lower the SOFC operating temperature to intermediate (500 °C – 750 °C) and low temperatures (300 °C – 500 °C) [6]. The literature commonly claims that at low operating temperatures, intracellular kinetic reactions slow down and the temperature–dependent electrical conductivity of the solid electrolyte decreases. Because of the poor ion conductive performance of the electrolyte, the great electrical efficiency attained at high temperatures is greater than at low temperatures. To compensate for this sudden loss in thermo–electrical efficiency, several researchers have moved to novel types of solid electrolyte synthesis research. Ytterbium–stable Zirconia (YSZ) type solid electrolytes are commonly used in today's SOFC units due to their structural and thermal resilience at high temperatures. [7, 8]. However, the electrical conductivity of YSZ decreases significantly at low operating temperatures. In contrast, Bismuth Oxide (Bi_2O_3)–based solid electrolyte systems, which are anticipated to be a good solid electrolyte option, exhibit greater electrical conductivity in the same temperature range as YSZ electrolytes [9, 10]. This situation has attracted the attention of many researchers who are studying on the synthesis and characterization of solid electrolyte materials. Many studies on Bi_2O_3 phases in the literature have found that the cubic δ–phase has the highest electrical conductivity of any solid electrolyte at comparable temperatures [11–15]. However, the stability of this phase in a relatively restricted temperature range (729 °C – 824 °C) throws doubt on these materials' solid electrolyte candidacy. Nevertheless, several successful studies have shown that this phase can be stabilized by doping rare earth oxides

(Ln_2O_3, Ln: Er, Eu, Dy, and so on) into the pure crystal. But, conductivity studies on this phase indicated that the stabilized phase's electrical conductivity was lower than that of the pure phase. This abrupt drop in conductivity is commonly attributed to the partial cation exchange associated with doping, which results in a loss in polarization power. Due to its $6s^2$ single electron chain, the host Bi^{3+} cation has a larger anion polarization power than the rare earth cations (Ln^{3+}) that replace itself [16]. In reality, a cation's polarizing power is related to its effective ion radius. As a result, using highly polarizable rare earth cations as dopants can help compensate for this dramatic drop in electrical conductivity [16, 17]. Many research on the stability of the cubic δ–phase, on the other hand, demonstrated that utilizing cations with lower radius for doping compared to the host Bi^{3+} (1.17 Å) cation yielded more successful results in stability studies. Otherwise, the rhombohedral crystal structure, which has lower electrical conductivity, is shown to become stable. In terms of doping strategy, studies using single, double, and triple doping methods yielded successful results in the literature, although the maximum electrical conductivity was obtained with the double doping method [18, 19].

The $(Bi_2O_3)_{1-x-y}$ $(Er_2O_3)_x(Tb_4O_7)_y$ ternary systems with doped two rare earth oxides were fabricated by solid state reactions at ambient temperature under air circumstances. The produced samples were structurally characterized using the X–Ray Diffraction (XRD) method, thermally characterized using the Thermo–gravimetry and Differential Thermal Analysis (TG&DTA) methodology, and electrically characterized using the Four Point End Technique (FPPT). Each characterization's results were compared to the others, and the data were interpreted individually in terms of the creation of the stable cubic δ–phase.

Materials and Methods

Sample Preparation

The high quality (> 99.0%) Bi_2O_3 ceramic powders and rare earth oxides (Er_2O_3, Tb_4O_7) were supplied from Sigma Aldrich Company. Under atmospheric circumstances, solid state reactions were used to create the desired $(Bi_2O_3)_{1-x-y}$ $(Er_2O_3)_x$ $(Tb_4O_7)_y$ ternary mixtures. The doping mole percentages were determined using a specific stoichiometry in order to investigate the effects of the doping ratio on the electrical conductivity and crystalline phase structure of the material. The additive mole percentages of $(Bi_2O_3)_{1-x-y}$ $(Er_2O_3)_x$ $(Tb_4O_7)_y$ triple solid mixtures are listed in Table 1. Powder chemicals were weighed using a precision digital scale before being crushed in an agate mortar with a pestle for about 25 minutes to obtain desirable dopant diffusion. The mixtures were then put in a programmed furnace utilizing heat–resistant alumina boats and annealed for 100 hours at 750 °C, which is temperature above the phase transition temperature (729 °C). This temperature was chosen to ensure that the cubic phase was the dominant phase all crystal structure for all temperatures and that the dopants diffused into the pure crystal more successfully. The annealed powder mixtures were then utilized to make disc–shaped pallet samples with a diameter of 13 mm and a thickness of 0.5 mm in order to conduct the XRD and conductivity tests. The pallet examples were created using a SPECAC type pressing machine, which can apply 10 tons of mechanical pressure along the vertical axis.

Table 1. Molar dopant ratios of $(Bi_2O_3)_{1-x-y}$ $(Er_2O_3)_x$ $(Tb_4O_7)_y$ ternary mixtures.

Samples	Molar dopant ratios of components		
	x : y (mol %)	Contents ratios (1: ↔ 5 %)	Total dopant concentration (mol %)
05Er05TbSB	05 : 05	1:1	10
05Er10TbSB	05 : 10	1:2	15
10Er05TbSB	10 : 05	2:1	15
15Er05TbSB	15 : 05	3:1	20
15Er10TbSB	15 : 10	3:2	25
20Er05TbSB	20 : 05	4:1	25
20Er10TbSB	20 : 10	4:2	30

Characterization Techniques

The samples' XRD patterns were created using a Panalytical Empyrean model X–ray diffractometer with a scanning step of 0.02°/s and a range of 10°< 2θ < 90°. To detect X–rays scattered from distinct atomic planes, a thallium (Ta)–activated sodium iodide detector (NaI) was employed. For scanning process, monochromatic X–rays with a wavelength of 1.54 Å generated by Cu–K_α radiation were utilized. The X–Powder and Win–Index software's were used to index diffraction patterns. All XRD patterns were superimposed in the scanned angle range to observe single phase stability. The Perkin Elmer Diamond model Thermogravimetric and Differential Thermal Analysis (TG & DTA) equipment was used to analyze the thermal behavior of the samples throughout a temperature range of 30 °C to 1000 °C with a constant heating rate of 10 °C/min. The obtained DTA curves were thoroughly examined to see whether a phase transition could occur during the uniform heating operation. Temperature dependent TGA curves, on the other hand, were considered to evaluate mass change. Finally, the FPPT was used to measure the temperature–dependent electrical conductivity of the samples. The conductivity measurements were carried out by heating the alumina kit system at a constant up from room temperature to about 950 °C in a controlled furnace. For measurements, four high–purity platinum wires with a diameter of 0.5 mm were used. Each of these platinum wires was touched on the pallet sample at 0.20 cm intervals, and the current and voltage values from two of the channels were measured. To properly determine the temperature, K–type thermal couples were placed quite close to the sample. Current and voltage data were measured using a Keithley 2400 DC power supply and a Keithley 2700 multimeter. The measurements' data were sent to the controlled computer environment using an electronic

interface card that followed the "General Purpose Interface Bus" (GPIB) standard.

Result and Discussions

X–Ray Diffraction Method

Fig. 1 depicts the superimposed XRD patterns generated at room temperature. On each diffraction pattern, the cubic δ–phase and monoclinic α–phase diffraction peaks are identified. As they only include cubic δ–phase peaks, samples 05Er05TbSB, 05Er10TbSB, and 15Er05TbSB were determined to be stable in a single phase, that is, homogeneous phase structure, according to the peak positions marked in Fig. 1. When the diffraction patterns of other samples are thoroughly examined, it is discovered that they include both α–phase and δ–phase peaks [20]. As a result, at room temperature, these samples have a mixed phase structure. Additionally, there is a relationship between the doping rate and the intensity of the α–phase peaks, which are mixed phase indicators. As a result, it can be said that number of α–phase peaks increase as the dopant ratio increases [21]. This reveals that the rare earth cations settled in the crystal lattice by the doping process not only do not replace the Bi^{3+} cation, but also settle at various ion centres, increasing the defect density. Based on this perspective, the crystal defect density of samples generated with a high doping ratio increases, and the scattering peaks on the diffraction pattern indicating the development of mixed phases may be increased. Also, according to the literature, when the doping ratio increases, the lattice stress increases and the crystal size decreases. This suggests that the doping level be kept as low as possible in order for stability studies to be successful [22, 23].

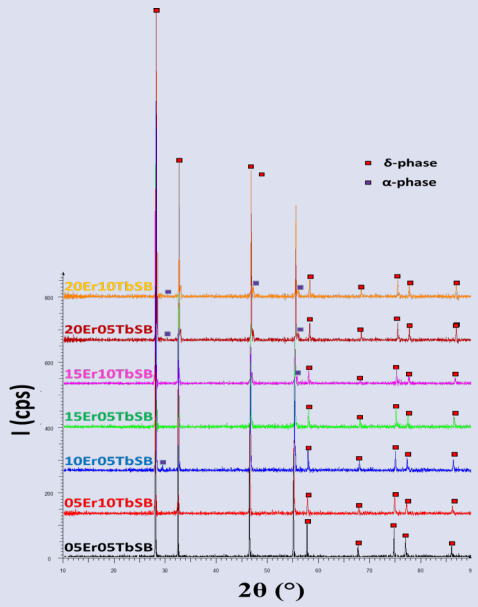

Figure 1. Superimposed XRD pattern of annealed samples at room temperature

Average crystal size and micro strain were determined using Eq. (1) and (2), respectively, for the lattice parameters.

$$D = \frac{k\lambda}{\beta cos\theta} \quad (1)$$

$$\epsilon = \frac{\beta}{4tan\theta} \quad (2)$$

The Scherrer formula is used to calculate crystal size in Eq. (1), where k is the shape factor, λ is the wavelength, β is the Fwhm value, and θ is the Bragg diffraction angle. The Stokes–Wilson formula is given in Eq. (2), where ε is the micro strain. Table 2 displays some of the estimated lattice parameters that have been related to the structural analysis results. Table 2 clearly shows the association between doping ratio and structural characteristics. The lattice constant of the samples stable with the cubic δ–phase is smaller than that of the pure cubic phase. The fundamental reason for this is because the rare earth cations that are doped into the lattice have a lower radius than the host Bi^{3+} cation. In the literature, this is referred to as lattice narrowing [24].

Table 2. Results of the structural analysis as well as the calculated lattice parameters.

Samples	Crystal structure parameters			
	Crystal size (nm)	Micro strain (%)	Crystal phase	Lattice constant
05Er05TbSB	78.2	0.0143	δ	5.512
05Er10TbSB	71.4	0.0167	δ	5.509
10Er05TbSB	73.2	0.0158	α, δ	Mixed
15Er05TbSB	65.1	0.0195	δ	5.493
15Er10TbSB	61.7	0.0221	α, δ	Mixed
20Er05TbSB	52.5	0.0216	α, δ	Mixed
20Er10TbSB	48.3	0.0326	α, δ	Mixed

Thermal Analysis

Fig. 2 shows temperature–dependent DTA and TGA curves for some manufactured samples. On the DTA curves, neither endothermic nor exothermic peak development was seen, indicating a probable phase transition, as shown in the figures. The temperature–dependent phase transition, in reality, begins with a change in crystal symmetry. According to the literature, the DTA curve for pure Bi_2O_3 powders reveals an endothermic peak at around 729 °C, suggesting the transition from the monoclinic α–phase to the cubic δ–phase.

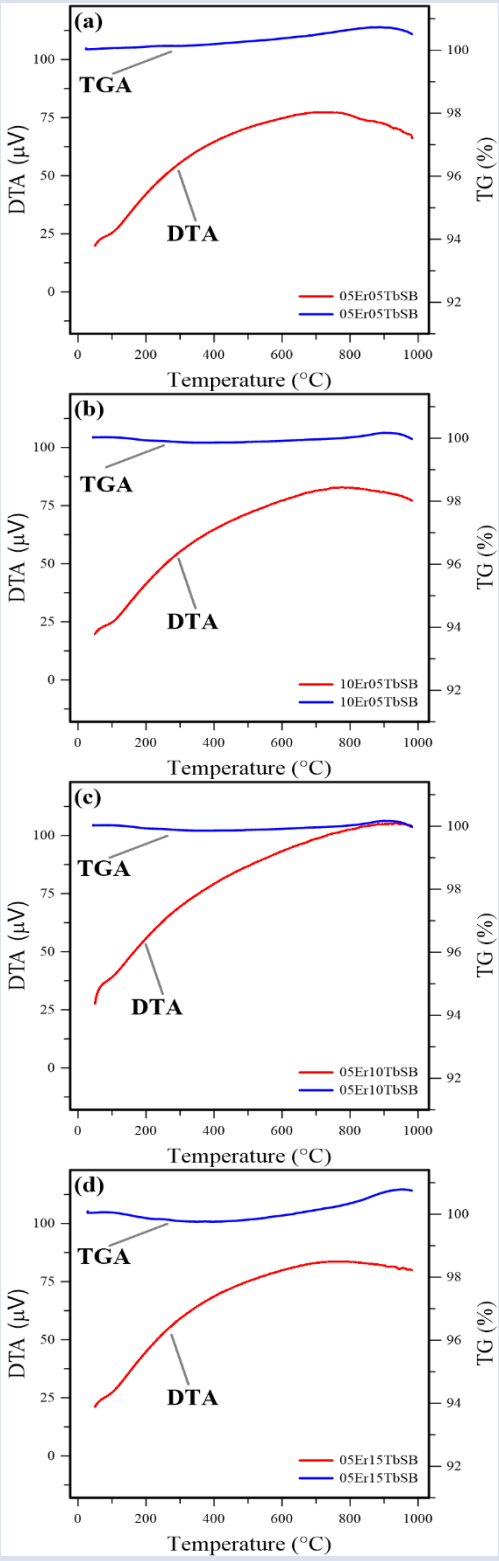

Figure 2. Temperature dependent DTA and TGA curves.

The lack of such a phase transition in our research for doped Bi_2O_3 powders can be ascribed to increasing lattice stress with doping. In other words, as a result of partial cation exchange, the dislocation density in the crystal lattice increases, preventing the lattice from transitioning to the lower symmetric crystal order [27]. Moreover, the DTA system's very fast heating rate might obscure a possible phase change. The heating rate used in this investigation was 10 °C/min, which may be insufficient for identifying phase transitions that produce minor temperature increases. The temperature–dependent TGA curves, on the other hand, reveal that mass losses are minimal. Mass losses in oxide–based ceramic systems, on the other hand, are commonly attributed to the removal of O_2 gas from the structure. Because the cation exchange caused by doping changes the polarization power. Besides, the Bi—O bonds are known to be stronger than Ln—O bonds, and this, together with doping, allows for the formation of additional oxygen anion vacancies in the lattice [28]. As a result of a chemical reaction, an O2– ion in the anion sublattice can be converted into the O_2 and therefore removed from the lattice. As a result, such reactions might be regarded as the principal cause of mass losses.

Conductivity Measurements

Fig. 3a shows the temperature–dependent conductivity graphs of the manufactured pallet samples. As seen in the graphs, increasing the doping rate results in a significant drop in conductivity. This is due to the partial cation exchange produced by the doping process between the host Bi^{3+} and Er^{3+} or Tb^{4+}.

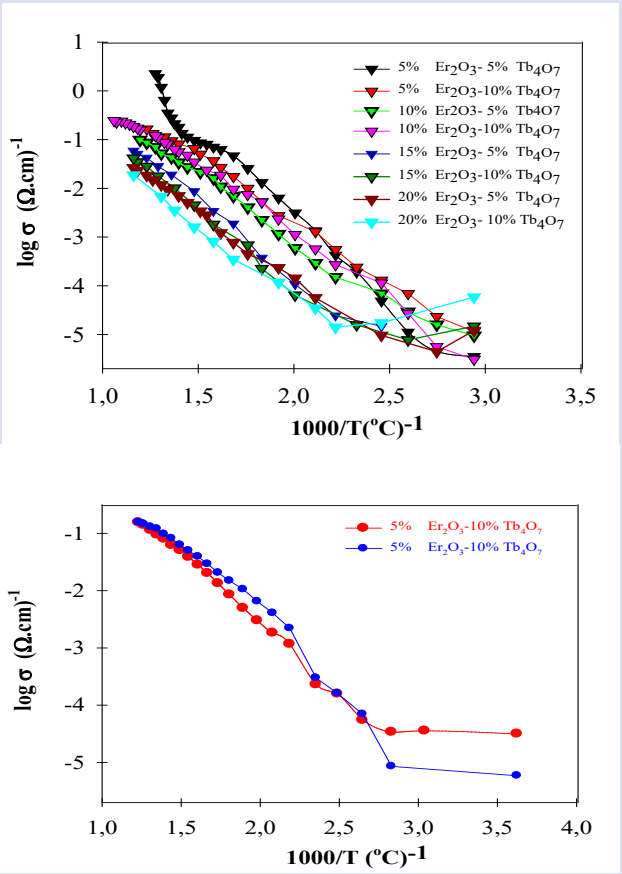

Figure 3. Arrhenius plots depending on temperature.

It is also well known that the Bi^{3+} cation has a strong polarization power, which is also described as the ability to disturb the anion sublattice. As a result, including rare earth cations into the lattice will result in a significant drop in polarization power. As a natural consequence, the conductivity curve of the 20Er05TSB sample generated with a high doping ratio is the lowest of all samples. In addition, as shown in the Fig.3a, the conductivity graph of sample 05Er05TbSB exhibits a sharp increase about 600 °C. This sudden increase in

conductivity is known as the order–disorder transition (ODT), which is a structural change in the oxygen sublattice of crystal system [29, 30]. With this ODT, some oxygen ions migrate from the regular 8c region to the octahedral regions known as 32f, which require less activation to jump to surrounding vacant ion centers. With this transition, the oxygen–ion mobility in the lattice accelerates, and the number of ions contributing to electrical conductivity increases significantly [31, 32]. On the other hand, the conductivity graph of sample 05Er10TbSB, whose heating (red) and cooling (blue) curves are shown in Fig. 3b. As seen in the graph, the change in conductivity with temperature follows the same trend. This demonstrates the chemical and structural stability of this sample when subjected to heat treatments. If you pay attention, the cooling conductivity curve has more conductivity than the heating conductivity curve. In fact, this is to be expected because the disorder–order transition becomes more difficult during cooling, and the consequences of high temperatures persist longer. The electrical activation energy were determined using the Arrhenius equation given by following equation.

$$\sigma_T = \sigma_0 \exp\left(-\frac{E_A}{k_B T}\right) \quad (3)$$

In equation (3), σ_T represents conductivity at any temperature, σ_0 represents conductivity at absolute temperature, E_A represents activation energy, and k_B represents the Boltzmann constant. Table 3 displays electrical activation energies derived from the conductivity graphs, as well as the conductivity values measured at 600 and 700 °C.

Table 3. Findings of conductivity measurements and electrical activation energies.

Samples	Conductivity measurement results		
	Conductivity at 600 °C $(\Omega.cm)^{-1}$	Conductivity at 700 °C $(\Omega.cm)^{-1}$	Activation Energy (eV)
05Er05TbSB	645E–4	128E–3	0.64
05Er10TbSB	269E–4	109E–3	0.73
10Er05TbSB	87.7E–4	36.2E–3	0.88
15Er05TbSB	27.1E–4	14.1E–3	0.92
15Er10TbSB	13.4E–4	65.6E–4	0.86
20Er05TbSB	8.51E–4	61.7E–4	1.02
20Er10TbSB	4.67E–4	28.6E–4	1.12

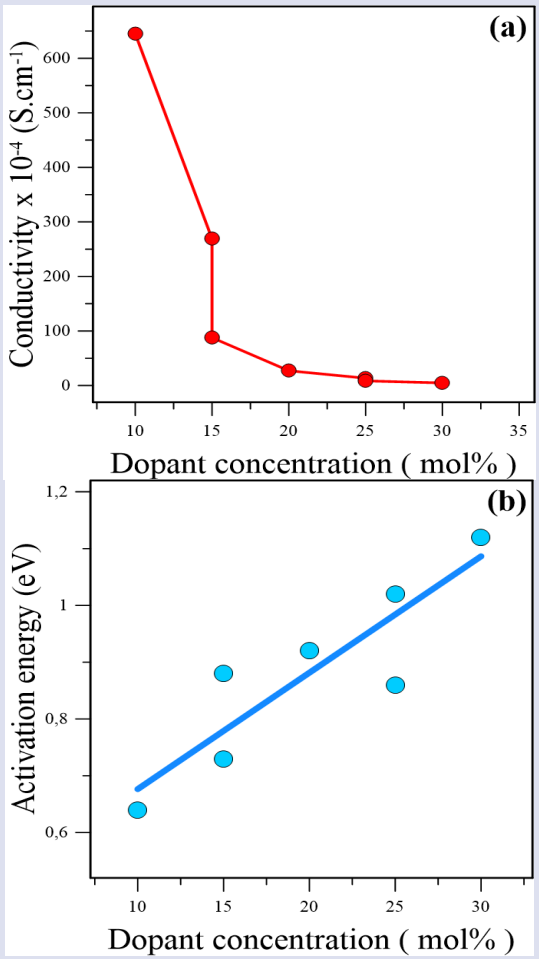

Figure 4. Activation energy and conductivity change according to doping concentration.

As seen in Table 3, as the doping ratio increases at the same temperature, the conductivity values drop while the activation energies increase. The activation energy is defined here as the lowest amount of energy necessary for an oxygen ion in the anion sublattice to hop to the unoccupied ion centers in the surrounding sublattice [33, 34]. As the doping ratio increases, so do the lattice dislocations, and rare earth cations introduced into the lattice can settle at lattice trap spots for oxygen ions [35]. The trapping of these O^{2-} ions, which are believed to contribute to ion conduction, increases the activation energy and, as a result, lowers conductivity.

Fig. 4a and b also depict how conductivity and activation energy change with doping ratio, respectively. The sample 05Er05TbSB created with the lowest doping ratio has the highest conductivity and the lowest activation energy, as seen in the figure. Low doping treatment can be regarded to be crucial in terms of reaching the maximum conductivity aim in stability investigations. In the case of heavy doping, on the other hand, the crystal lattice creates a large activation energy and so shows low electrical conductivity [36]. It has been underlined that the doping ratio should be kept as low as possible in order to produce stability and high electrical conductivity in research that employ the double doping technique and are also included in the literature. Jung et

al produced the binary operation $(Bi_2O_3)_{1-x-y}$ $(Dy_2O_3)_x$ $(WO_2)_y$ and attained the highest conductivity for a low doping of 12%. Furthermore, they proposed that by fixing this doping ratio, a 2:1 (Dy:W) dopant content ratio was efficient in reaching the greatest conductivity (0.57 $S.cm^{-1}$ at 700 °C) [37].

Conclusion

In this study, solid state reactions were used to create $(Bi_2O_3)_{1-x-y}$ $(Er_2O_3)_x$ $(Tb_4O_7)_y$ ternary systems, which were then characterized using XRD, TGA&DTA, and FPPT techniques. The effects of doping ratio on phase stability were clearly demonstrated by XRD data. Among all samples, the XRD diffraction pattern of 05Er05TbSB, 05Er10TbSB, and 15Er05TbSB indicated cubic δ–phase stability. Other samples, on the other hand, were discovered to exhibit mixed phase structure because their diffraction patterns showed monoclinic α–phase related peaks. Because the temperature dependent DTA curves did not show the creation of an endothermic or exothermic peak, which implies a phase transition, it was determined that the synthesized materials were thermally stable in the studied temperature range. The temperature–dependent conductivity graphs revealed that the doping ratio affected the electrical conductivity mechanism significantly. As a result, the sample with the lowest doping had the maximum conductivity at 700 °C, measuring 0.128 $S.cm^{-1}$. Furthermore, the activation energy determined on the conductivity curve of this sample was 0.64 eV, the lowest. These findings suggest that increasing lattice dislocation in samples produced with a high doping ratio shortens ion conduction channels and resulting in a substantial increase in activation energy. Because of the variation in polarizability of rare earth cations, it was assumed that the conductivity measurements acquired were lower than 0.57 S/cm^{-1}, the maximum conductivity value in the literature.

Conflicts of interest

There are no conflicts of interest in this work.

References

[1] Zakaria Z., Mat Z.A., Hassan S.H.A., Kar Y.B., A review of solid oxide fuel cell component fabrication methods toward lowering temperature, *Int. J. Energy Res.*, 44 (2020) 594–611.

[2] Azizi M.A., Brouwer J., Progress in solid oxide fuel cell–gas turbine hybrid power systems: System design and analysis, transient operation, controls and optimization, *Appl. Energy.*, 215 (2018) 237–289.

[3] Mahato N., Banerjee A., Gupta A., et al, Progress in material selection for solid oxide fuel cell technology: A review, *Prog. Mater. Sci.*, 72 (2015) 141–337.

[4] Singh M., Zappa D., Comini E., Solid oxide fuel cell: Decade of progress, future perspectives and challenges, *Int. J. Hydrog.*, 46 (2021) 27643–27674.

[5] Güldeste A., Aldoori M., Balci M., et al., Synthesis and characterization of Dy–Eu–Tm co–doped cubic phase stabilized bismuth oxide based electrolytes in terms of intermediate temperature–solid oxide fuel cells (IT–SOFCs), *J. Rare Earths.*, 41(3) 2023 406–412.

[6] Wachsman E. D., Lee K.T., Lowering the Temperature of Solid Oxide Fuel Cells, *Science,* 334 (2011) 935–939.

[7] Azad A.M., Larose S., Akbar S.A., Bismuth oxide–based solid electrolytes for fuel cells, *J. Mater. Sci.*, 29(1994) 4135–4151.

[8] Arı M., Balcı M., Polat Y., Synthesis and characterization of (Bi2O3)1−x−y−z(Gd2O3)x (Sm2O3)y(Eu2O3)z quaternary solid solutions for solid oxide fuel cell, *Chin. J. Phys.*, 56 (2018) 2958–2966.

[9] Ozlu H.T., Cakar S., Ersoy E., et al.,The bulk electrical conductivity properties of d–Bi2O3 solid electrolyte system doped with Yb2O3, *J. Therm. Anal. Calorim.*, 122 (2015) 525–536.

[10] Dilpuneet S., Aidhy J.C., Susan B.N., et al., Vacancy–Ordered Structure of Cubic Bismuth Oxide from Simulation and Crystallographic Analysis, *J. Am. Ceram. Soc.*, 91 (2008) 2349–2356.

[11] Jung D.W., Juan C.N., Duncan K.L., et al., Enhanced long–term stability of bismuth oxide–based electrolytes for operation at 500 °C, *Ionics*, 16 (2010) 97–103.

[12] Arasteha S., Maghsoudipour A., Alizadeh M., et al., Effect of Y2O3 and Er2O3 co–dopants on phase stabilization of bismuth oxide, *Ceram. Int.*, 37 (2011) 3451–3455.

[13] Bandyopadhyay S., Dutta A.A., Structural insight into the electrical properties of Dy–Ho co–doped phase stabilized Bismuth Oxide based electrolytes, *J. Electroanal. Chem.*, 817 (2018) 55–64.

[14] Cardenas P.S., Ayala M.T., Muñoz J., et al.,High ionic conductivity dysprosium and tantalum Co–doped bismuth oxide electrolyte for low–temperature SOFCs, *Ionics*, 26 (2020) 4579–4586.

[15] Tran T.B., Navrotsky A., Energetics of Dysprosia–Stabilized Bismuth Oxide Electrolytes, *Chem. Mater.*, 24 (2012) 4185–4191.

[16] Wachsman E. D., Boyapati S., Jiang N., Effect of dopant polarizability on oxygen sublattice order in phase–stabilized cubic bismuth oxides, *Ionics*, 7 (2001) 1–6.

[17] Jung D.W., Lee K.T., Wachsman E.D., Dysprosium and Gadolinium Double Doped Bismuth Oxide Electrolytes for Low Temperature Solid Oxide Fuel Cells, *J. Electrochem. Soc.*, 163 (2016) 411–415.

[18] Wachsman E.D., Boyapati S., Kaufman M.J., et al., Modeling of Ordered Structures of Phase–Stabilized Cubic Bismuth Oxides, *J. Am. Chem. Soc.*, 83 (2004) 1964–1968.

[19] Wang X., Zhou W., De Lisio J.B., et al., Doped δ–bismuth oxides to investigate oxygen ion transport as a metric for condensed phase thermite ignition, *Phys. Chem. Chem. Phys.*, 19 (2017) 12749–12758.

[20] Jaiswal N., Gupta B., Kumar D., et al., Effect of addition of erbium stabilized bismuth oxide on the conductivity of lanthanum doped ceria solid electrolyte for IT–SOFCs, *J. Alloys Compd.*, 633 (2015) 174–182.

[21] Trana T.B., Navrotsky A., Energetics of disordered and ordered rare earth oxide–stabilized bismuth oxide ionic conductors, *Phys. Chem. Chem. Phys.*, 16 (2014) 2331–2337.

[22] Kış M., Polat Y., Erdoğan B., et al., New fabricated electrolytes based on Dy3+–Tm3+ double–doped δ–Bi2O3–type cubic phase, *J. Aust. Ceram. Soc.*, 56 (2020) 987–993.

[23] Kuo Y.L., Liu L.D., Lin S.E., et al., Assessment of structurally stable cubic Bi12TiO20 as intermediate temperature solid oxide fuels electrolyte, *J. Eur. Ceram*., 31 (2011) 3119–3125.

[24] Rivera O.D., Martínez A., Rodil S.E., Interpretation of the Raman spectra of bismuth oxide thin films presenting different crystallographic phases, *J. Alloys Compd*., 853 (2021) 157245.

[25] Hou J., Bi L., Qian J., Zhu Z., et al., Study of the Crystal Structures of New Buffer Materials Bi 1−x Y x O 1.5. J. Supercond, *Nov. Magn.*, 23 (2010) 1011–1014.

[26] Yogamalar R., Srinivasan R., Vinu A., et al., X–ray peak broadening analysis in ZnO nanoparticles, Solid State Commun., 149 (2009) 1919–1923.

[27] Koçyiğit S., Gökmen Ö., Temel S., et al., Structural investigation of boron undoped and doped indium stabilized bismuth oxide nanoceramic powders, *Ceram. Int*., 39 (2013) 7767–7772.

[28] Bandyopadhyay S., Dutta A., Thermal, optical and dielectric properties of phase stabilized δ – Dy–Bi2O3 ionic conductors, *J. Phys. Chem. Solids*., 102 (2015) 12–20.

[29] Torun H.O., Çakar S., Thermal characterization of Er–doped and Er–Gd co–doped ceria–based electrolyte materials for SOFC, *J. Therm. Anal. Calorim*., 133 (2018) 1233–1239.

[30] Jung D.W., Duncan K.L., Wachsman E.D., Effect of total dopant concentration and dopant ratio on conductivity of (DyO1.5)x–(WO3)y–(BiO1.5)1−x−y, *Acta Mater*., 58 (2010) 355–363.

[31] Painter A.S., Huang Y.L., Wachsman E.D, Durability of (La0.8Sr0.2)0.95MnO3–δ–(Er0.2Bi0.8)2O3 composite cathodes for low temperature SOFCs, *J. Power Sources*., 360 (2017) 391–398.

[32] Jiang N., Wachsman E.D., Structural Stability and Conductivity of Phase–Stabilized Cubic Bismuth Oxides, *J. Am. Ceram. Soc*., 82 (1999) 3057–3064.

[33] Aytimur A., Koçyiğit S., Uslu İ., et al., Fabrication and characterization of bismuth oxide–holmia nanofibers and nanoceramics, *Curr. Appl. Phys*., 13 (2013) 581–58.

[34] Chou T., Liu L.D., Wei W.C.J., Phase stability and electric conductivity of Er2O3–Nb2O5 co–doped Bi2O3 electrolyte, *J. Eur. Ceram*., 31 (2011) 3087–3094.

[35] Panuh D., Ali S.A.M., Yulianto D., et al., Effect of yttrium–stabilized bismuth bilayer electrolyte thickness on the electrochemical performance of anode–supported solid oxide fuel cells, *Ceram. Int*., 47 (2021) 6310–6317.

[36] Wachsman E.D., Effect of oxygen sublattice order on conductivity in highly defective fluorite oxides, *J. Eur. Ceram. Soc*., 24 (2004) 1281–1285.

[37] Fruth V., Ianculescu A., Berger D., et al., Synthesis, structure and properties of doped Bi2O3, *J. Eur. Ceram. Soc*., 26 (2006) 3011–3016.